A molecular simulation analysis of producing monatomic carbon chains by stretching ultranarrow graphene nanoribbons

2010 Nanotechnology 21 265702

(http://iopscience.iop.org/0957-4484/21/26/265702)

Nanotechnology **21** (2010) 265702 (7pp) doi:10.1088/0957-4484/21/26/265702

A molecular simulation analysis of producing monatomic carbon chains by stretching ultranarrow graphene nanoribbons

Zenan Qi[1], Fengpeng Zhao[1], Xiaozhou Zhou[1], Zehui Sun[1], Harold S Park[2] and Hengan Wu[1,3]

[1] Department of Modern Mechanics, CAS Key Laboratory of Materials Behavior and Design, University of Science and Technology of China, Hefei, Anhui 230027, People's Republic of China
[2] Department of Mechanical Engineering, Boston University, Boston, MA 02215, USA

E-mail: wuha@ustc.edu.cn

Received 23 March 2010, in final form 15 May 2010
Published 4 June 2010
Online at stacks.iop.org/Nano/21/265702

Abstract

Atomistic simulations were utilized to develop fundamental insights regarding the elongation process starting from ultranarrow graphene nanoribbons (GNRs) and resulting in monatomic carbon chains (MACCs). There are three key findings. First, we demonstrate that complete, elongated, and stable MACCs with fracture strains exceeding 100% can be formed from both ultranarrow armchair and zigzag GNRs. Second, we demonstrate that the deformation processes leading to the MACCs have strong chirality dependence. Specifically, armchair GNRs first form DNA-like chains, then develop into monatomic chains by passing through an intermediate configuration in which monatomic chain sections are separated by two-atom attachments. In contrast, zigzag GNRs form rope-ladder-like chains through a process in which the carbon hexagons are first elongated into rectangles; these rectangles eventually coalesce into monatomic chains through a novel triangle–pentagon deformation structure under further tensile deformation. Finally, we show that the width of GNRs plays an important role in the formation of MACCs, and that the ultranarrow GNRs facilitate the formation of full MACCs. The present work should be of considerable interest due to the experimentally demonstrated feasibility of using narrow GNRs to fabricate novel nanoelectronic components based upon monatomic chains of carbon atoms.

S Online supplementary data available from stacks.iop.org/Nano/21/265702/mmedia

(Some figures in this article are in colour only in the electronic version)

1. Introduction

With the ongoing development of both micro-and nanoelectromechanical systems (M/NEMS) and the resulting miniaturization of electronic devices, there has recently been extensive interest in studying the properties of molecular and atomic scale components. For example, devices where electrons hop onto, and off from, a single atom between two contacts would be the ultimate limit. Because of this, creating reliable and stable single atom chains has long become the focus of research in this field. Experimental studies where a monatomic chain of several Au atoms (Au atom chain of single atom width) pulled out were first reported in 1998 [1, 2]. In 2003, long linear carbon chains inserted in multiwalled carbon nanotubes were observed [3, 4].

However, interest in the field has shifted dramatically with the recent discovery of graphene, the world's only known two-dimensional (2D) material [5, 6]. In particular, because of

[3] Author to whom any correspondence should be addressed.

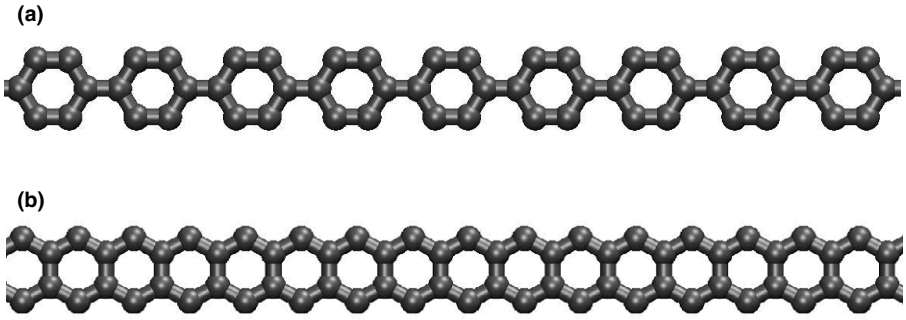

Figure 1. Schematic diagram of the narrowest possible GNR for (a) an armchair GNR (AGNR) and (b) a zigzag GNR (ZGNR).

its remarkable conductivity and other exceptional physical, chemical, and electronic properties, including nanometric dimensions, quantized conductance, high modulus of elasticity, unusual optical features, and electromagnetic response [5–10], graphene is a promising candidate to be fabricated as an M/NEMS component.

Recently, graphene nanoribbons (GNRs) whose width is smaller than about 20 nm have been derived both by chemical synthesis and irradiation methods [11–13]; we note that the GNRs were found to exist stably without hydrogen termination by Jin *et al* [11]. GNRs are of particular interest due to the fact that graphene has been found to become a semiconductor once the width of the GNR becomes smaller than about 20 nm [14, 15]. With regards to the present work, GNRs are relevant because monatomic carbon chains (MACCs) can easily be produced by the elongation of narrow GNRs, as shown in previous works [16, 17]. Furthermore, single atomic chains containing more than ten carbon atoms have been observed to have a lifetime spanning hundreds of seconds [11]; in contrast, metallic atom chains have been experimentally observed to become unstable after timescales on the order of seconds [1]. Recent experimental studies have also shown that MACCs derived from graphene have exceptional promise as conductors due to their outstanding stability and electrical properties [18–20].

Previous atomistic simulations have shown that MACCs can be obtained by pulling GNRs with graphene leads [16]; however, these studies did not analyze or elucidate the mechanisms underlying the elongation process. Furthermore, the critical effect of GNR chirality was also not considered. Finally, these studies did not demonstrate the importance of using the narrowest GNR to achieve very stable MACCs with high fracture strains exceeding 100% under tensile loading.

Therefore, it is the objective of the present work to, using molecular dynamics (MD), molecular mechanics (MM), and density functional theory (DFT) simulations, analyze and shed light onto the factors controlling the elongation process of ultranarrow (i.e. single unit cell wide) GNRs. We first demonstrate that highly elongated and stable MACCs are possible from both ultranarrow armchair and zigzag nanoribbons. We then demonstrate that chirality plays a critical role in the resulting elongation process, where ultranarrow armchair and zigzag GNRs exhibit a significantly different mechanical response due to the operant deformation mechanisms under tensile loading. Finally, the results suggest that the formation of complete and elongated MACCs is greatly facilitated by being pulled from ultranarrow GNRs; this critical point was not observed by previous GNR deformation studies [21, 22]. These results should be of technological relevance due to the extensive interest in using carbon-based materials, including MACCs, as the building blocks for novel nanoelectronics and M/NEMS [15].

2. Model and methodology

A schematic diagram of the two different GNRs considered in the present work is shown in figure 1; snapshots for this and all subsequent figures were taken using VMD, a visualization tool to view MD simulation results [23]. In our work, the MD simulations were performed using LAMMPS [24], while the carbon–carbon interactions were modeled using the adaptive intermolecular reactive empirical bond order (AIREBO) potential [25]. The AIREBO potential has been shown to accurately capture the bond–bond interaction between carbon atoms as well as bond breaking and bond re-forming. The cutoff distance for the REBO part of the potential was set within LAMMPS to be 2 Å to avoid spuriously high bond forces during the fracture process, as described by Shenderova *et al* [26]. The time step was chosen as 1 fs, and the simulations were carried out at room temperature (300 K) in an *NVT* ensemble. The GNRs were stretched using tensile loading by applying a ramp displacement that went from zero in the middle of the GNR to a maximum value at the two axial ends of the GNR. The strain rate in the simulations was set as 10^8 s^{-1}, or equivalently 0.5 m s^{-1}; we note that this is much slower than the upper bound speed of 30 m s^{-1} found by Wang *et al* for MACC formation [16, 19]. The MD and MM simulations were utilized to examine the details of the tensile evolution process, while DFT calculations were utilized to examine the energetic stability of the various GNR and MACC configurations.

3. Simulation details and results

We first establish that complete MACC formation is possible from both ultranarrow AGNRs and ZGNRs; we will examine the atomistic details of the chirality-dependent MACC formation later. The ultranarrow AGNR we considered in figure 1(a) had a length of 54.954 Å, with periodic boundary

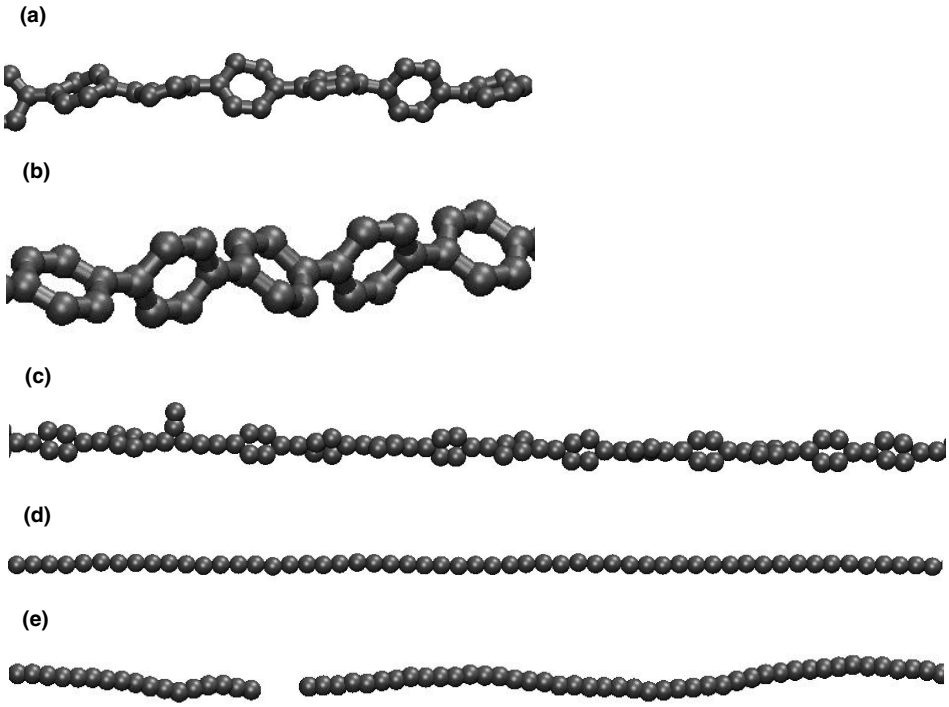

Figure 2. (a) DNA-like AGNR during relaxation, (b) another angle of the DNA-like AGNR, (c) the appearance of MACCs with multiple atom attachments at a strain of 35%, (d) complete transformation of the AGNR into an MACC at a strain of 133% and (e) fracture of the MACC at a strain of 150%.

conditions (PBC) in the length direction to mimic an infinitely long AGNR, and had free surfaces in the transverse directions such that finite width effects could be considered. A conjugate gradient (CG)-based energy minimization was first carried out at 0 K before dynamic, tensile loading was applied at room temperature as described above; snapshots of the AGNR during the elongation process are seen in figure 2.

During the initial equilibration, the AGNR demonstrated a rotation and distortion of the initially planar structure, as some of the hexagons have rotated out of their initial planes, as seen in figures 2(a) and (b); this rotation and distortion occurs due to the edge stress induced warping, as discussed by Shenoy *et al* [27]. Specifically, the carbon–carbon bond connecting adjacent hexagons acts as an axis, about which each six-atom hexagon ring rotates. Some of the adjacent hexagon rings are observed to be nearly perpendicular, and the entire AGNR assumes a DNA-like chain.

After a tensile strain of 20%, the hexagon unit cells became significantly deformed, as a noticeable elongation of the six-atom hexagons was observed. By a strain of 35%, MACCs with multiple atom attachments were observed as in figure 2(c); these MACCS then continued to elongate under further tensile loading. The multiple atom attachments existed due to the inability to completely and instantaneously pull all atoms of a six-atom hexagon ring into the MACC; the last (highly distorted) six-atom hexagon persisted until a strain of 85.5%. Furthermore, at a strain of 133%, all multiple atom attachments were absorbed into the MACC, thus forming a long and complete MACC, as seen in figure 2(d). The average distance between neighboring atoms was 1.64 Å, with a range from 1.46 to 1.72 Å. Under continuing stretching, the bond lengths increased and finally fracture of the MACC was observed at a strain of 150%, as in figure 2(e).

MM simulations of the same AGNR model were also performed by CG energy minimization. In these MM simulations, tensile strain was applied by fixing one end of the AGNR, prescribing a displacement of 0.05 Å at the other end, allowing the interior atoms to relax to energy minimizing configurations, and repeating. Note that due to the fact that the MM simulations were performed at 0 K, the AGNR showed little of the rippling that was observed in figure 2 at room temperature. A similar tensile evolution process was observed for the MM simulations as compared to MD, including alternating vertical units due to rotation and buckling of adjacent hexagons, reconstruction to MACCs, and fracture. More importantly, the MM simulations revealed that energy minimization was responsible for the twisted configuration seen in figures 2(a) and (b). Specifically, the DNA-like structure in figure 2(a) had a potential energy that was about 0.68% lower than the initial, undeformed configuration seen in figure 1(a), i.e. the twisted configuration enables the AGNR to relieve the stresses that result from the armchair edges [27].

We studied the energetics of the MACC configurations using both DFT and MM simulations. In the DFT calculations, an infinite MACC model was established with PBC in all three directions, though in the two transverse directions, the periodic distances were set much larger than 10 Å to ensure no interactions between MACCs. We utilized the generalized gradient approximation (GGA) for the exchange correlation functional [28] in the CASTEP code [29], where

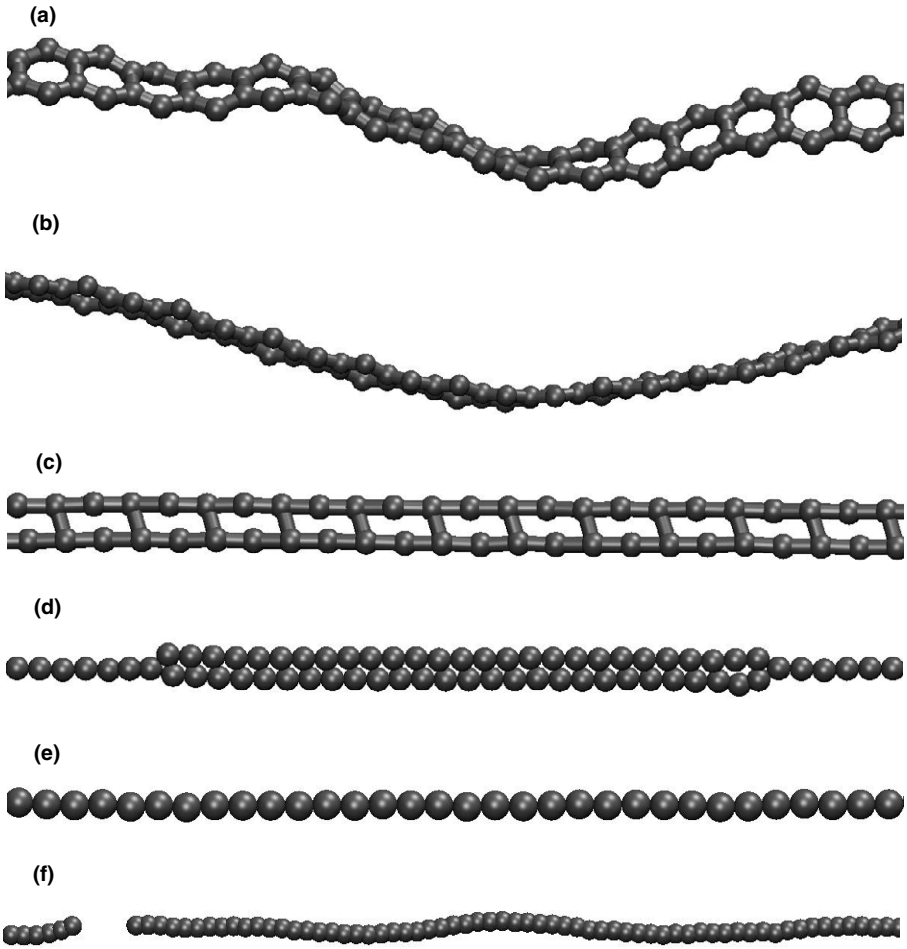

Figure 3. (a) Rope-ladder-like ZGNR during relaxation, (b) elimination of thermally induced fluctuations after energy minimization, (c) hexagonal to rectangular deformation at a strain of 42.5%, (d) multiple MACCs at a strain of 77%, (e) formation of complete MACC from ZGNRs at a strain of 180% and (f) fracture of the MACC at a strain of 188.5%.

the energy cutoff was 400 eV and the k-point mesh was set to $1 \times 1 \times 21$ to ensure more than 10 k-points in the length direction. After optimization, it was found through the DFT calculations that the MACC indeed existed in a stable configuration, and contained bonds with lengths of 1.261 and 1.301 Å, respectively. The results are comparable to those of the previous MD simulations after fracture where an average bond length of 1.341 Å was found.

In the MM simulation, we studied a MACC with 100 atoms. The model was considered without PBCs in the axial direction, so we consider bond lengths in the middle of the MACC only to avoid any edge or surface effects. After applying an initial random velocity to generate a representative finite temperature profile, the CG method was applied to find the minimum energy configuration of the MACC. Before energy minimization, three bond lengths were dominant; those bond lengths were 1.12, 1.42 and 1.62 Å. However, after energy minimization, all the bond lengths were found to have a double bond length of 1.332 Å, which is very close to the average DFT bond length of 1.281 Å and MD bond length of 1.341 Å. The results also justify the usage of the classical AIREBO potential for studying MACCs.

To study the effect of chirality on the deformation processes leading to MACCs, we also studied the tensile deformation of ZGNRs. As seen in figure 1(b), the connection between adjacent six-atom hexagons for ZGNRs is accomplished using two carbon atoms, as compared to just one atom for the AGNR; therefore, it is expected that the rotation and twist that was observed for the AGNR in figure 2(a) may not be observed for ZGNRs.

The atomistic model used for the ZGNR was similar to the AGNR, and had a total length of 48.944 Å, with PBC applied along the axial direction, while free surfaces were allowed along the transverse directions to examine the effects of finite width. The ZGNR was first relaxed by energy minimization, then an MD simulation was performed using the same linear ramp displacement profile as was used to apply tensile deformation to the AGNR; the deformation process for the ZGNR is shown in figure 3.

Interestingly, during relaxation, the ZGNR acted as a suspended rope ladder, as shown in figure 3(a), which again results from relieving the edge stress that results from the zigzag edges [27]. While the entire ZGNR wrinkled significantly, the hexagon rings showed little rotation and

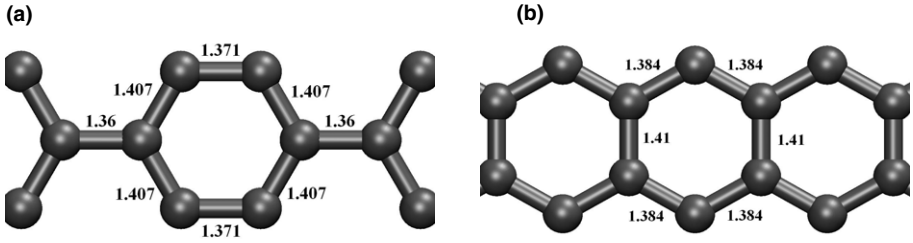

Figure 4. Bond lengths of (a) AGNR and (b) ZGNR after energy minimization (Å).

instead formed a parallel rope-ladder-like ribbon in which atoms at the edges of the cross direction had nearly the same height, though when thermal fluctuations are discarded in the MM energy minimization simulations, the minimum energy configuration of figure 3(a) is one in which the parallel edges of the hexagon remain planar, as seen in figure 3(b).

As can be seen in figure 3, the processes and mechanisms enabling the eventual formation of a MACC from the ZGNR are completely different than those seen in figure 2 for the AGNR. In particular, the major deformation process was a reorientation and elongation of the six-atom hexagons initially seen in figure 3(a) to six-atom rectangles as seen in figure 3(c). Furthermore, it could be seen that the atoms at the edges form an angle of nearly 180°, as compared to the 120° angle observed for the initial, undeformed hexagons. In fact, when all of the hexagons had transformed into rectangles, as in figure 3(c), the original ZGNR essentially became two parallel lines of atoms.

With further elongation, the two parallel rows of atoms coalesced into a single row of atoms after a tensile strain of 42.5%, as observed in figure 3(d), where the MACCs surrounded the two parallel rows of atoms in the center of the ZGNR. We note the similarity of this structure to the multiple atom attachments that were observed during the tensile deformation of AGNR in figure 2(c), which again results from the inability to completely and instantaneously pull all atoms that comprise the rectangular structure seen in figure 3(c) into the MACC. Finally, at a strain of 180%, the ZGNR had completely become a MACC, and the MACC fractured eventually at a strain of 188.5%. The results in figures 2(d) and 3(e) suggest that very long and stable MACCs can be derived under tensile loading from both ultranarrow AGNRs and ZGNRs.

Table 2 summarizes the strain values between AGNRs and ZGNRs for configurations of interest. Specifically, it shows that MACCs are first seen at different strains for the AGNR and ZGNR, i.e. 35% for the AGNR as compared to 42% for the ZGNR; both the AGNR and ZGNR exhibit large fracture strains of 150% and 188%, respectively. In our simulations, the averaged and maximum bond lengths just before fracture are 1.761 and 1.781 Å for AGNR, 1.712 and 1.790 Å for ZGNR.

We now examine in detail the specific atomistic deformation mechanisms that enable both the AGNR and ZGNR to form MACCs under tensile loading. Importantly, we will show how chirality effects have a first order effect on the observed deformation mechanisms leading to the MACCs

Table 1. Data comparison of AGNR and ZGNR models.

Chirality	Length (Å)	Number of atoms	Total potential energy (eV)	Potential energy per C atom (eV)
AGNR	54.954	78	−452.254	−5.798
ZGNR	48.944	80	−490.761	−6.135

Table 2. Data comparison of critical strains during the tensile elongation of AGNR and ZGNR. Strain A is the strain when the MACC was first observed, strain B is the strain when the entire GNR formed a MACC, and strain C is the fracture strain.

Chirality	Original length (Å)	Strain A (%)	Strain B (%)	Averaged bond length at B (Å)	Strain C (%)	Averaged bond length at C (Å)
AGNR	54.954	35	133	1.642	150	1.761
ZGNR	48.944	42	180	1.712	188	1.764

for both AGNR and ZGNR. We first briefly discuss the bond lengths in the AGNR, as shown in figure 4(a); this is done because it is known for covalently bonded materials that the longer covalent bonds tend to be weaker.

A detailed analysis of the deformation mechanism starting with an undeformed AGNR and ending up with a MACC is shown in figures 5(a)–(c). There, it could clearly be observed that in going from the six-atom hexagon ring in figure 5(a) to the intermediate two-atom configuration in figure 5(b), failure initiated with the two weaker 1.407 Å bonds in figure 4(a), which were pulled first into the MACC. It is also due to these weaker 1.407 Å bonds that the AGNR initiates the MACC formation at a smaller strain level (35%) as compared to ZGNR (42%), as shown in table 2. Subsequent to the incorporation of the two long 1.407 Å bonds in the AGNR, the remainder of the two-atom configuration in figure 5(b) was pulled into the MACC under continued tensile loading.

In contrast, the ZGNR underwent a significantly different elongation process, as observed in figure 6. There, we first saw the buckling of the initially six-atom hexagon in figure 6(a) to the elongated rectangle in figure 6(b), as previously discussed. Under continued tensile loading, the elongated rectangles in figure 6(b) began to form a MACC, as shown in figure 6(c), with a very unusual deformation mechanism. In particular, it was observed that the rectangle joined the MACC by rotating the bond that connects the two parallel lines of carbon atoms in figure 6(b), which formed a triangle–pentagon structure behind the MACC, as seen in figure 6(c). Upon further tensile loading,

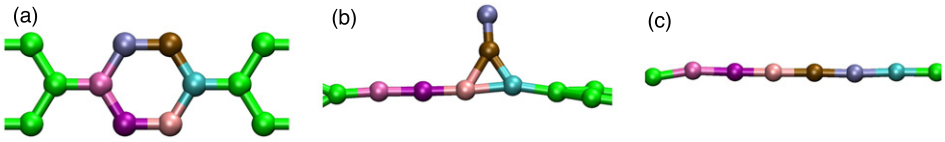

Figure 5. (best viewed in color) Elongation process from initial AGNR in (a) to intermediate configuration in (b) to MACC in (c).

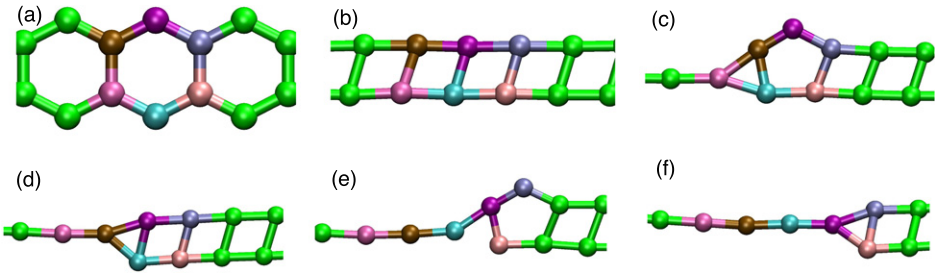

Figure 6. Illustration of MACC formation through the triangle–pentagon structure under tensile loading for the ZGNR (best viewed in color; note the colors represent the same atoms of the AGNR in figure 5 as for the ZGNR in this figure).

the bond in the triangle that was nearly orthogonal to the tensile loading direction (which connects the brown and light blue atoms in figure 6(c)) rotated in the direction of the tensile loading, and joined the MACC, as seen in figure 6(d), leaving a triangular structure in front of the elongated rectangles. Interestingly, subsequent deformation processes demonstrated, as seen in figures 6(e) and (f), that the triangle–pentagon deformation mechanism remained operative, and controlled the subsequent elongation of the remainder of the non-MACC portion of the ZGNR into the MACC. Specifically, the transition between figures 6(d) and (e) illustrates that the pentagon formation is energetically favorable as it is not possible to pull both bonds of the triangle in figure 6(d) into the MACC simultaneously; as one of the triangular bonds is pulled into the MACC in figure 6(e), the other dangling bond from the triangle in figure 6(d) forms a pentagon with the rectangle directly connected to it in figure 6(e) to minimize the system potential energy during the bond breaking process. To verify our simulation method, the energy is computed for different deformation stages using both MD and DFT. More information is available in a supplementary information file (available at stacks.iop.org/Nano/21/265702/mmedia).

Our atomistic simulation results clearly show that full MACCs that consist of only single carbon atoms can be obtained from the tensile deformation of the narrowest (single unit cell wide) AGNR and ZGNR. We emphasize that MACC formation has not been observed in previous atomistic simulations of the tensile deformation of wider GNRs before fracture [21, 22, 30, 31]. In contrast, in the MD simulations of Wang *et al* [16, 17], a MACC was obtained from a larger GNR; however, they utilized an idealized initial configuration in which a single atom contact bridging two pieces of a wider GNR was used as a seed to form the MACC. Furthermore, upon elongation, only a small portion of the wider GNR was drawn into the MACC.

Our results are also consistent with the experimental studies of MACC formation of Jin *et al* [11], who used controlled electron irradiation to thin GNRs to eventually form MACCs. Furthermore, it was noted in the work of Jin *et al* [11] that MACC formation should be possible from both AGNRs and ZGNRs, which has been shown in our work. Furthermore, they calculated that the formation energy for MACCs decreases as the width of the GNR decreases; this is also consistent both with the previous atomistic simulations [21, 22, 30, 31], where MACC formation was not found from the tensile deformation of wider GNRs, but also with our current work. Specifically, we performed MD simulations of the tensile elongation of 2-AGNR (two unit cells wide) and 2-ZGNR; the 2-ZGNR elongated to a MACC, while the 2-AGNR fractured at a strain of 50%, where no MACC formation was observed. All of these results taken together strongly suggest that a combination of GNR chirality and width is critical for the formation of full MACCs.

4. Conclusions

Our atomistic simulations have shown that elongated monatomic chains of carbon atoms can be pulled from ultranarrow GNRs. More importantly, we have demonstrated that the chirality of the GNR has a significant influence on both the deformation mechanisms that are observed during the tensile loading, and the failure properties of the resulting monatomic carbon chain, as the hexagon rings of the nanoribbons were shown to exhibit distinct chirality-dependent deformation patterns and fracture characteristics. Finally, in comparison with previous atomistic studies on MACC formation [11, 16, 17] we have shown the utility of using ultranarrow (i.e. single unit cell wide) GNRs to achieve elongated and stable MACCs of atoms with fracture strains exceeding 100%. Due to the current ability to experimentally synthesize narrow GNRs with tailored edge functionality [32], the present results suggest that researchers may be able to exploit their distinct properties under tensile loading to create unique and novel components for future M/NEMS.

Acknowledgments

This research was supported by the National Basic Research Program of China under grant No. 2006CB300404 and NSF China under grant No. 10902107.

References

[1] Ohnishi H, Kondo Y and Takayanagi K 1998 Quantized conductance through individual rows of suspended gold atoms *Nature* **395** 780–3
[2] Yanson A I, Bollinger G R, van den Brom H E, Agrait N and van Ruitenbeek J M 1998 Formation and manipulation of a metallic wire of single gold atoms *Nature* **395** 783–5
[3] Liu Y, Jones R O, Zhao X L and Ando Y 2003 Carbon species confined inside carbon nanotubes: A density functional study *Phys. Rev.* B **68** 125413
[4] Zhao X L, Ando Y, Liu Y, Jinno M and Suzuki T 2003 Carbon nanowire made of a long linear carbon chain inserted inside a multiwalled carbon nanotube *Phys. Rev. Lett.* **90** 187401
[5] Geim A K 2009 Graphene: status and prospects *Science* **324** 1530–4
[6] Geim A K and Novoselov K S 2007 The rise of graphene *Nat. Mater.* **6** 183–91
[7] Larade B, Taylor J, Mehrez H and Guo H 2001 Conductance, I–V curves, and negative differential resistance of carbon atomic wires *Phys. Rev.* B **64** 075420
[8] Wang Y, Huang Y H, Yang B H and Liu R Z 2006 Structural and electronic properties of carbon nanowires made of linear carbon chains enclosed inside zigzag carbon nanotubes *Carbon* **44** 456–62
[9] Alkorta I and Elguero J 2006 Theoretical study of the bond energy in *n*-silanes and *n*-germanes: comparison with *n*-alkanes *Chem. Phys. Lett.* **429** 58–61
[10] Fantini C *et al* 2006 Resonance Raman study of linear carbon chains formed by the heat treatment of double-wall carbon nanotubes *Phys. Rev.* B **73** 193408
[11] Jin C H, Lan H P, Peng L M, Suenaga K and Iijima S 2009 Deriving carbon atomic chains from graphene *Phys. Rev. Lett.* **102** 205501
[12] Xiang H J, Kan E J, Wei S H, Whangbo M H and Yang J L 2009 'Narrow' graphene nanoribbons made easier by partial hydrogenation *Nano Lett.* **9** 4025–30
[13] Son Y W, Cohen M L and Louie S G 2006 Energy gaps in graphene nanoribbons *Phys. Rev. Lett.* **97** 216803
[14] Han M Y, Ozyilmaz B, Zhang Y B and Kim P 2007 Energy band-gap engineering of graphene nanoribbons *Phys. Rev. Lett.* **98** 206805
[15] Chen Z H, Lin Y M, Rooks M J and Avouris P 2007 Graphene nano-ribbon electronics *Physica* E **40** 228–32
[16] Wang Y, Lin Z Z, Zhang W X, Zhuang J and Ning X J 2009 Pulling long linear atomic chains from graphene: molecular dynamics simulations *Phys. Rev.* B **80** 233403
[17] Wang Y, Ning X J, Lin Z Z, Li P and Zhuang J 2007 Preparation of long monatomic carbon chains: molecular dynamics studies *Phys. Rev.* B **76** 165423
[18] Hu Y H 2009 Stability of sp carbon (carbyne) chains *Phys. Lett.* A **373** 3554–7
[19] Mikhailovskij I M, Wanderka N, Ksenofontov V A, Mazilova T I, Sadanov E V and Velicodnaja O A 2007 Preparation and characterization of monoatomic C-chains: unraveling and field emission *Nanotechnology* **18** 475705
[20] Chen W, Andreev A V and Bertsch G F 2009 Conductance of a single-atom carbon chain with graphene leads *Phys. Rev.* B **80** 085410
[21] Lu Q and Huang R 2009 Nonliear mechanics of single-atomic-layer graphene sheets *Int. J. Appl. Mech.* **1** 443–67
[22] Zhao H, Min K and Aluru N R 2009 Size and chirality dependent elastic properties of graphene nanoribbons under uniaxial tension *Nano Lett.* **9** 3012–5
[23] Humphrey W, Dalke A and Schulten K 1996 VMD: visual molecular dynamics *J. Mol. Graph.* **14** 33–8
[24] Plimpton S 1995 Fast parallel algorithms for short-range molecular-dynamics *J. Comput. Phys.* **117** 1–19
[25] Stuart S J, Tutein A B and Harrison J A 2000 A reactive potential for hydrocarbons with intermolecular interactions *J. Chem. Phys.* **112** 6472–86
[26] Shenderova O A, Brenner D W, Omeltchenko A, Su X and Yang L H 2000 Atomistic modeling of the fracture of polycrystalline diamond *Phys. Rev.* B **61** 3877–88
[27] Shenoy V B, Reddy C D, Ramasubramaniam A and Zhang Y W 2008 Edge-stress-induced warping of graphene sheets and nanoribbons *Phys. Rev. Lett.* **101** 245501
[28] Perdew J P, Chevary J A, Vosko S H, Jackson K A, Pederson M R and Singh D J 1992 Atoms, molecules, solids, and surfaces—applications of the generalized gradient approximation for exchange and correlation *Phys. Rev.* B **46** 6671–87
[29] Segall M D, Lindan P J D, Probert M J, Pickard C J, Hasnip P J and Clark S J 2002 First-principles simulation: ideas, illustrations and the CASTEP code *J. Phys.: Condens. Matter* **14** 2717–44
[30] Bu H, Chen Y F, Zou M, Yi H, Bi K D and Ni Z H 2009 Atomistic simulations of mechanical properties of graphene nanoribbons *Phys. Lett.* A **373** 3359–62
[31] Gao Y W and Hao P 2009 Mechanical properties of monolayer graphene under tensile and compressive loading *Physica* E **41** 1561–6
[32] Jia X T, Hofmann M, Meunier V, Sumpter B G, Campos-Delgado J and Romo-Herrera J M 2009 Controlled formation of sharp zigzag and armchair edges in graphitic nanoribbons *Science* **323** 1701–5